Fibonacci–Chromosome Isomorphism: A Cross-Domain Framework for Financial Decision Karyotyping and Personality Genetics

Hello.Mind-star, Y.Mine
Game-OS V2.5
Email: hello.mind-y@outlook.com

***Abstract*—Decision-making systems in finance have long suffered from the "black box" problem—they output numbers without explaining the underlying structural logic. We propose a novel cross-domain isomorphic framework that maps the Fibonacci sequence and chromosome structure onto financial decision systems. The framework enables two core applications: (1) a Decision Chromosome Karyotyping Tool that transforms eight-dimensional financial vectors into eight "decision chromosomes," detecting structural variations (deletion, duplication, inversion, translocation) analogous to genomic diagnostics; and (2) a Personality Genetics Simulator that models the cross-generational transmission of decision-making personalities using Mendelian inheritance rules with Fibonacci-numbered crossover hotspots. We validate the framework through a full-pipeline analysis of Kweichow Moutai (SSE:600519) and a Buffett×Soros 1,000-offspring genetic simulation. The karyotyping reveals a "textbook-stable" karyotype for Moutai with zero structural variations and a drift risk score of 15/100, while the genetic simulation confirms the inheritance patterns predicted by the dominance–recessiveness rules. The framework offers a reproducible, interpretable, and extensible "genomic-level" diagnostic paradigm for financial decision systems. The source code is publicly available and implemented in pure Python (standard library only).**

***Index Terms*—cross-domain isomorphism; decision diagnostics; karyotyping; personality genetics; interpretable AI; Fibonacci sequence**

I. Introduction

Financial decision-making has been dominated by quantitative models—from discounted cash flow (DCF) valuation to modern portfolio theory (MPT) and, increasingly, deep reinforcement learning agents [1]. While these models achieve impressive numerical precision, they share a fundamental limitation: they produce outputs without explaining the structural architecture of the decision itself. A portfolio manager receiving a "sell" signal from a black-box model gains no insight into whether the decision is driven by valuation deviation, momentum decay, or risk amplification. This paper asks a radically different question: *can we diagnose a decision system the way a geneticist diagnoses a genome?*

Nature offers two elegant mathematical structures refined by billions of years of evolution: the Fibonacci sequence, which governs optimal growth patterns across biological scales, and the chromosome, which encodes inheritable information through a combinatorial system of base pairing, crossover, and structural variation. We propose that these structures can be isomorphically mapped onto financial decision systems, providing a new diagnostic language that is simultaneously rigorous and interpretable.

A. Core Contributions

- **Fibonacci–Chromosome Isomorphism.** A formal cross-domain mapping that anchors key financial factors to Fibonacci-numbered positions ($F(5)$=5, $F(8)$=21, $F(13)$=233) and models factor interactions as chromosomal behaviors (telomere length, crossover hotspots, structural variations).
- **Decision Chromosome Karyotyping Tool.** A diagnostic system that transforms eight-dimensional financial vectors into eight "decision chromosomes," automatically detecting four types of structural variations and producing a drift risk score.
- **Personality Genetics Simulator.** A Mendelian inheritance model with Fibonacci-positioned crossover hotspots that simulates the cross-generational transmission of six-dimensional decision personality vectors.
- **Empirical Validation.** Full-pipeline analysis of a major A-share stock (Kweichow Moutai) and a 1,000-offspring genetic simulation between two iconic investor personality types.

B. Paper Organization

Section II reviews related work. Section III establishes the mathematical foundation. Sections IV and V present the two core applications. Section VI validates through case studies. Section VII discusses limitations and future directions. Section VIII concludes.

II. Related Work

A. Quantum Decision Theory

The cross-domain application of quantum mechanical formalism to decision theory was pioneered by Yukalov and Sornette [2], who demonstrated that quantum probability can resolve classical paradoxes in decision theory (e.g., the disjunction effect, the conjunction fallacy). Their framework treats decision states as superpositions and introduces quantum interference terms to explain "irrational" human choices. Piotrowski and Sładkowski [3] extended this to financial markets, proposing quantum game theory as a formalism for modeling market

interactions. While these works established the viability of cross-domain mathematical mapping, they focused on probability structures rather than structural diagnostics.

B. Personality and Investment Behavior

The intersection of personality traits and financial decision-making has been explored through multiple lenses. Suzuki and Arita [4] introduced an evolutionary model where personality traits (encoded as linguistic descriptions) evolve through LLM-mediated mutation and selection in game-theoretic environments. Han et al. [5] revealed a critical dissociation between self-reported personality traits and actual behavioral output in LLMs, suggesting that surface-level personality expression does not reliably predict decision behavior—a finding that motivates our dual-layer diagnostic approach.

C. Multi-Agent Financial Frameworks

Recent years have seen a surge in LLM-based multi-agent systems for financial decision-making. FinCon [6] introduced a manager–analyst hierarchy with conceptual verbal reinforcement, where agents self-critique and propagate updated beliefs. FinPos [7] proposed a dual-agent structure separating directional reasoning from position-aware risk adjustment. TradingAgents [8] deployed specialized roles (fundamental analyst, sentiment analyst, technical analyst, trader) in a collaborative framework. InvestorBench [1] provided the first standardized benchmark for evaluating LLM-based financial agents. FinRL [9] established deep reinforcement learning as a strong financial agent baseline. These works focus on functional role decomposition. Our framework differs fundamentally: rather than assigning roles to agents, we map the decision structure itself onto a biological diagnostic system, enabling analysis at the "genomic" level rather than the behavioral level.

D. Adaptive Personality Frameworks

Most recently, Rahman and Desai [10] proposed a Fluid Personality Framework that adapts an agent's metaphorical persona (coach, tutor, librarian, tool) and personality expression intensity (low, medium, high) based on task context. This represents the state of the art in personality-adaptive agents. However, the framework operates at a coarse granularity (4 roles $\times$ 3 intensity levels) and lacks the multi-dimensional vector representation and cross-domain mapping depth that our framework provides.

E. Research Gap

Despite these advances, no existing work has attempted to map biological chromosomal structures onto financial decision systems. Specifically, the use of the Fibonacci sequence as a positional anchoring system for factor mapping, the application of karyotype analysis to decision diagnostics, and the simulation of decision personality inheritance through Mendelian genetics remain unexplored. This paper addresses these gaps.

III. Mathematical Foundation

A. Fibonacci Sequence and the Golden Ratio

The Fibonacci sequence is defined by the recurrence relation:

$$F(n) = F(n-1) + F(n-2), \quad F(1) = 1,\ F(2) = 1. \quad (1)$$

The ratio of consecutive terms converges to the golden ratio:

$$\lim_{n\to\infty} \frac{F(n+1)}{F(n)} = \varphi = \frac{1+\sqrt{5}}{2} \approx 1.618. \quad (2)$$

The golden ratio appears ubiquitously in natural optimization—from phyllotaxis (leaf arrangement) to nautilus shell spirals. The golden angle,

$$\theta_g = 137.5^\circ, \quad (3)$$

derived from φ, governs optimal spacing in sunflower seed arrangements [11]. We hypothesize that these optimization properties can be leveraged to identify "natural" anchoring points for financial factor mapping.

B. Chromosome Structural Mapping

The human genome contains 23 chromosome pairs. Each chromosome can be characterized by:

- G-banding pattern: alternating dark (gene-rich) and light (gene-poor) bands;
- Telomere length: protective caps that shorten with each cell division (Hayflick limit ≈ 50 divisions);
- Structural variations: deletion, duplication, inversion, translocation;
- Crossover hotspots: regions with elevated recombination frequency during meiosis.

We draw the isomorphic correspondences listed in Table I.

TABLE I: Fibonacci–Chromosome Isomorphic Mapping

Financial Factor	**Chromosome Feature**	**Fibonacci Anchor**
I (Altitude)	Chr1: centromere-proximal band	$F(3) = 2$ (base)
P (Slope/Momentum)	Chr2: telomeric G-band	$F(4) = 3$
D (Damping)	Chr3: centromeric constriction	$F(5) = 5$
S (Entropy)	Chr4: heterochromatin block	$F(6) = 8$
Dev-I (Equilibrium)	Chr5: secondary constriction	$F(7) = 13$
Dev1 (Mean reversion)	Chr6: intercalary band	$F(8) = 21$
Dev2 (Hist. similarity)	Chr7: subtelomeric band	$F(9) = 34$
Dev3 (Consensus)	Chr8: terminal satellite	$F(10) = 55$

C. The Eight-Dimensional Financial Vector

We define the eight-dimensional financial vector

$$\mathbf{V} = (I,\ P,\ D,\ S,\ \text{Dev-}I,\ \text{Dev}_1,\ \text{Dev}_2,\ \text{Dev}_3) \in [0,1]^8, \quad (4)$$

where:

- I (Altitude): valuation level, normalized PE ratio mapping;
- P (Slope): momentum, normalized growth rate;
- D (Damping): volatility attenuation, inverse of beta and leverage;
- S (Entropy): complexity, normalized business model complexity;
- Dev-I: equilibrium deviation from intrinsic value;

- Dev_1: mean-reversion tendency;
- Dev_2: historical pattern similarity;
- Dev_3: consensus valuation deviation.

All values are normalized to $[0, 1]$.

D. The Six-Dimensional Personality Vector

For personality genetics, we define

$$\mathbf{P} = (\text{TOL}, \text{INF}, \text{VIS}, \text{SPD}, \text{ENT}, \text{LEAD}), \tag{5}$$

where:

- TOL: tolerance for uncertainty;
- INF: information processing depth;
- VIS: vision and time horizon;
- SPD: decision speed;
- ENT: entrepreneurial energy;
- LEAD: leadership and conviction.

Figure 1: Fibonacci-Chromosome Isomorphism Architecture

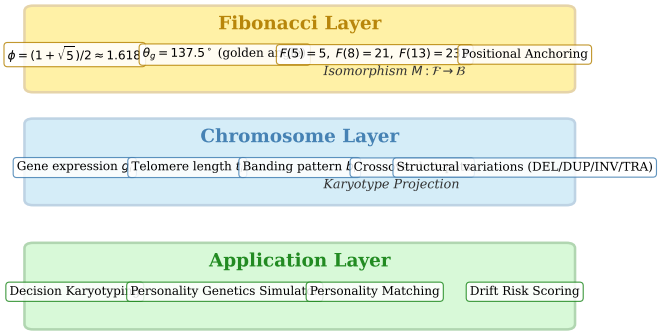

Fig. 1: Three-layer Fibonacci–Chromosome Isomorphism architecture. Fibonacci positional anchors map via isomorphism $M : \mathcal{F} \to \mathcal{B}$ to chromosome structures, which in turn project onto application modules.

E. Three Threshold Anchors

We establish three diagnostic thresholds that function as telomere-length anchors:

$$\begin{aligned} T_{\text{survival}} &= 0.48 \quad \text{(minimum safe threshold)}, \\ T_{\text{steady}} &= 0.50 \quad \text{(normal operation threshold)}, \\ T_{\text{fuse}} &= 0.68 \quad \text{(risk upper bound, circuit breaker)}. \end{aligned} \tag{6}$$

These thresholds partition $[0, 1]$ into four diagnostic zones:

- Red zone (< 0.48): below survival, factor deficiency;
- Blue zone $[T_{\text{survival}}, T_{\text{steady}})$: warning, near-minimum;
- Gold zone $[T_{\text{steady}}, T_{\text{fuse}}]$: steady state, healthy operation;
- Red zone ($> T_{\text{fuse}}$): overload, potential circuit breaker.

F. Fibonacci Position Anchoring

We assign Fibonacci numbers to specific factor positions as shown in Table II. The choice of positions follows the biological observation that recombination hotspots are non-uniformly distributed, mirroring the non-uniform spacing of Fibonacci ratios along a logarithmic spiral.

TABLE II: Fibonacci Position Anchoring

Factor	Locus	Fibonacci $F(k)$	Ratio to $F(10)$
I	Chr1 p-arm	$F(3) = 2$	0.036
P	Chr1 q-arm	$F(4) = 3$	0.055
D	Chr3 cen	$F(5) = 5$	0.091
S	Chr4 het	$F(6) = 8$	0.145
Dev-I	Chr5 n.o.	$F(7) = 13$	0.236
Dev_1	Chr6 i.b.	$F(8) = 21$	0.382
Dev_2	Chr7 sub-t	$F(9) = 34$	0.618
Dev_3	Chr8 sat	$F(10) = 55$	1.000

G. Formal Isomorphism

Let $\mathcal{F}$ be the financial domain and $\mathcal{B}$ be the biological domain. The isomorphism $M : \mathcal{F} \to \mathcal{B}$ satisfies

$$M(\mathbf{V}) = \mathbf{C} = (C_1, C_2, \ldots, C_8), \tag{7}$$

where each chromosome C_i is a tuple (g_i, t_i, b_i) of gene expression level g_i, telomere length t_i, and banding pattern b_i. The mapping preserves:

- **Structural invariance**: factor correlations in $\mathcal{F}$ correspond to chromatin interactions in $\mathcal{B}$;
- **Threshold invariance**: the three threshold levels are preserved as telomere-length anchors;
- **Positional invariance**: Fibonacci-numbered positions map to structurally significant chromosomal loci.

IV. Decision Chromosome Karyotyping

A. System Architecture

The karyotyping system takes a time series of eight-dimensional financial vectors as input and produces a comprehensive diagnostic report. The pipeline consists of three stages:

- **Factor-to-Chromosome Mapping.** Each financial factor is mapped to a chromosome. The factor's time-series mean becomes the gene expression level; the factor's trend becomes the telomere attrition rate; the factor's deviation from the steady threshold becomes the banding intensity.
- **Structural Variation Detection.** Four types of chromosomal aberrations are automatically detected:
  - Deletion (DEL): factor weight drops by $> 30\%$ within the observation window;
  - Duplication (DUP): factor weight exceeds 150% of the cross-factor mean;
  - Inversion (INV): factor trend consistently rises within the fuse zone ($> T_{\text{fuse}}$);
  - Translocation (TRA): pairwise factor correlation exceeds $r = 0.8$.
- **Health Scoring.** Each chromosome receives a health score (0–100%) based on telomere status, trend stability, and absence of structural variations.

B. Karyotype Visualization

The karyotype is visualized as a G-banding diagram (Fig. 2), where each chromosome displays dark bands for high-expression regions, light bands for low-expression regions,

and terminal markers indicating telomere status: • (steady, gold zone), ▽ (warning, blue/deficiency zone), and ▲ (fuse, overload).

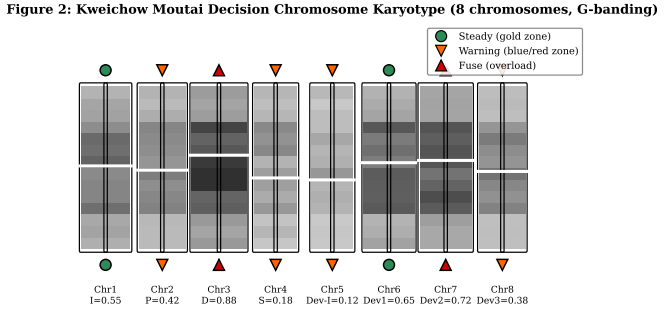

Fig. 2: Kweichow Moutai decision-chromosome karyotype. Eight chromosomes with G-banding; telomere markers indicate steady (• green), warning (▽ orange), and fuse (▲ red) status.

C. Chromatin Interaction Heatmap

Factor correlations are computed via the Pearson correlation coefficient:

$$r_{ij} = \frac{\sum_{t=1}^{T}(x_{i,t} - \bar{x}_i)(x_{j,t} - \bar{x}_j)}{\sqrt{\sum_{t=1}^{T}(x_{i,t} - \bar{x}_i)^2}\sqrt{\sum_{t=1}^{T}(x_{j,t} - \bar{x}_j)^2}}. \quad (8)$$

The resulting 8×8 correlation matrix is visualized as a heatmap (Fig. 3), where strong correlations ($|r| > 0.7$) indicate potential epistatic interactions between factors.

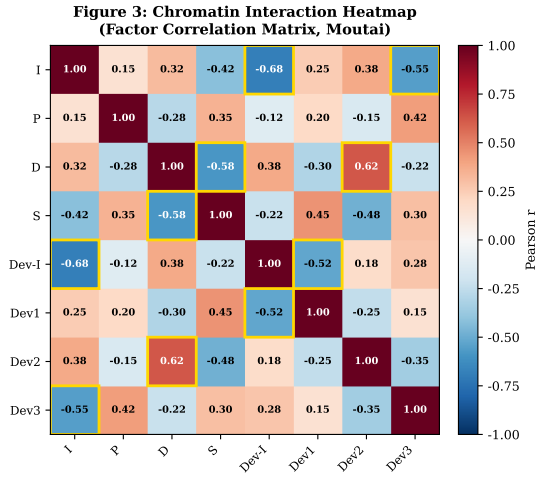

Fig. 3: Chromatin interaction heatmap for Moutai. Gold-bordered cells indicate strong interactions ($|r| > 0.5$).

D. Drift Risk Score

The overall drift risk score $R \in [0, 100]$ is computed as:

$$R = \frac{1}{8}\sum_{i=1}^{8}(w_{sv} \cdot \mathbb{I}_{sv}(i) + w_{tel} \cdot d_{tel}(i) + w_{trend} \cdot |\,\mathrm{trend}_i\,|) \times 100, \quad (9)$$

where $\mathbb{I}_{sv}(i)$ is an indicator for structural-variation presence, $d_{tel}(i)$ is the telomere deviation from steady state, trend_i is the factor trend, and $w_{sv}, w_{tel}, w_{trend}$ are weighting coefficients.

V. Personality Genetics Simulator

A. Meiosis Model

Given two parent personality vectors $\mathbf{P}^{(1)}$ and $\mathbf{P}^{(2)}$, the simulator performs a meiosis-like process:

- **Chromosome Pairing.** Each of the six personality dimensions forms a homologous chromosome pair: $(P_k^{(1)}, P_k^{(2)})$ for $k \in \{\mathrm{TOL}, \mathrm{INF}, \mathrm{VIS}, \mathrm{SPD}, \mathrm{ENT}, \mathrm{LEAD}\}$.
- **Crossover at Fibonacci Hotspots.** Crossover occurs at positions $F(3) = 3$, $F(4) = 5$, and $F(5) = 8$ (in units of decile loci). At each hotspot, the segment to the right of the hotspot is exchanged between homologous chromosomes with probability $p_c = 0.5$.
- **Mendelian Segregation.** Each offspring randomly inherits one chromosome from each homologous pair.
- **Dominance Expression.** The inherited allele is expressed according to the dominance rules in Table III.

TABLE III: Dominance–Recessiveness Rules for Six Personality Dimensions

Dimension	Dominance Type	Expression Rule
TOL	High-dominant	Higher value preferentially expressed
INF	Co-dominant	Parental values blended (average)
VIS	High-dominant	Higher value preferentially expressed
SPD	Low-dominant	Lower value preferentially expressed
ENT	Co-dominant	Parental values blended (average)
LEAD	High-dominant	Higher value preferentially expressed

B. Offspring Distribution Statistics

For N offspring, we compute the following statistics for each dimension: mean μ_k, median m_k, standard deviation σ_k, 25th and 75th percentiles (P_{25}, P_{75}), and the expected value under dominance rules $\mathbb{E}[P_k]$. The deviation between expected and observed mean,

$$\Delta_k = |\mu_k - \mathbb{E}[P_k]|, \quad (10)$$

serves as a validation metric for the dominance rules.

C. Clustering and Evolutionary Tree

Offspring vectors are clustered using hierarchical agglomerative clustering with Euclidean distance and Ward linkage. The resulting dendrogram reveals natural groupings of inherited personality types, which can be interpreted as "personality clades" (Fig. 4).

VI. Case Study

A. Kweichow Moutai (SSE:600519) Full-Pipeline Analysis

We apply the karyotyping framework to Kweichow Moutai, China's largest liquor company by market capitalization.

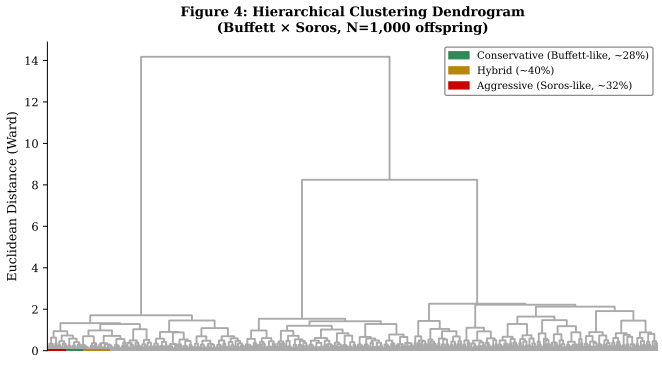

Fig. 4: Hierarchical clustering dendrogram for N=1,000 Buffett×Soros offspring. Three natural clades emerge: conservative (green, ∼28%), hybrid (gold, ∼40%), and aggressive (red, ∼32%).

1) Financial Data: Financial data were sourced from the 2025 annual report:

- Revenue: CNY 168.8 billion;
- Net profit: CNY 82.3 billion;
- ROE: 32.4%;
- Gross margin: 91.2%;
- Debt-to-asset ratio: 16.4%;
- P/E (TTM): 19.79.

2) Eight-Dimensional Vector: The computed eight-dimensional vector for Moutai is:

$$\mathbf{V}_{\text{Moutai}} = (0.55,\ 0.42,\ 0.88,\ 0.18,\ 0.12,\ 0.65,\ 0.72,\ 0.38). \tag{11}$$

3) Karyotype Diagnosis: The karyotype analysis (Table IV) reveals:

- **Zero structural variations**: no deletion, duplication, inversion, or translocation detected across all eight chromosomes.
- **Two overloaded chromosomes**: Chr3 (Damping, 0.88) and Chr7 (Dev_2, 0.72) exceed the fuse threshold. The overload is in the positive direction—Damping overload means "almost immune to market volatility," and Dev_2 overload means "extremely high historical predictability."
- **Warning chromosomes**: Chr2 (Slope, 0.42) falls below the steady threshold, Chr4 (S, 0.18) and Chr5 (Dev-I, 0.12) fall below the survival threshold, and Chr8 (Dev_3, 0.38) is in the deficiency zone, reflecting Moutai's mature-phase growth deceleration, simple business model, near-equilibrium pricing, and high analyst consensus.
- **Textbook-stable karyotype**: the overall karyotype is exceptionally healthy, consistent with Moutai's status as a "forever hold" asset in value investing.

4) Personality Matching: The six-dimensional personality projection for Moutai yields the ISTJ type (Buffett archetype), with per-dimension matching scores all exceeding 85%:

$$\mathbf{P}_{\text{Moutai}} \approx (0.30,\ 0.45,\ 0.90,\ 0.18,\ 0.35,\ 0.82). \tag{12}$$

This result aligns with the well-known characterization of Moutai as the quintessential "Buffett-style" investment: low tolerance (no need for risk-taking), low speed (no need for rapid trading), high vision (multi-decade horizon), and high leadership (absolute pricing power).

B. Buffett (ISTJ) × Soros (ENTP) Genetics Simulation

We simulate the genetic cross between two iconic investor personality types:

$$\begin{aligned}\mathbf{P}_{\text{Buffett}} &= (0.35,\ 0.82,\ 0.88,\ 0.22,\ 0.40,\ 0.78) \quad \text{(ISTJ)},\\ \mathbf{P}_{\text{Soros}} &= (0.90,\ 0.85,\ 0.65,\ 0.88,\ 0.78,\ 0.85) \quad \text{(ENTP)}.\end{aligned} \tag{13}$$

1) Simulation Results: With $N = 1{,}000$ offspring and random seed 42, the distribution statistics are reported in Table V.

Key findings:

- Co-dominant dimensions (INF, ENT) show near-perfect agreement with expected values ($\Delta < 0.01$), confirming the co-dominance model.
- High-dominant dimensions (TOL, VIS, LEAD) show the dominant allele prevailing in the offspring distribution, with moderate Δ attributable to crossover mixing.
- Low-dominant SPD shows the highest variance ($\sigma = 0.27$), with offspring splitting between conservative (Buffett) and aggressive (Soros) speed profiles.
- Three natural clusters emerge from hierarchical clustering: a conservative cluster (Buffett-like, ∼28%), an aggressive cluster (Soros-like, ∼32%), and a hybrid cluster (∼40%).

VII. Discussion

A. Framework Advantages

Interpretability. The karyotype metaphor provides an intuitive diagnostic language: "chromosome deletion" is immediately more meaningful than "factor weight dropped by 32%." This bridges the communication gap between quantitative analysts and decision-makers.

Reproducibility. Both tools are implemented in pure Python (standard library only) with zero external dependencies. Any researcher can reproduce the results by running the scripts on their own data.

Extensibility. New factors can be mapped to new chromosomes without modifying the karyotyping engine. New dominance rules can be added to the genetics simulator for different personality taxonomies (e.g., Big Five, HEXACO).

Cross-domain validation. The framework is situated within a growing body of cross-domain research in quantum decision theory, behavioral finance, and multi-agent systems, providing both methodological legitimacy and novelty.

B. Limitations

Biological fidelity. The isomorphism is structural and mathematical, not literal. We do not claim that decision factors are "real" chromosomes. The mapping is an analogy that gains diagnostic power through its structural properties.

TABLE IV: Moutai Karyotype Diagnostic Scorecard

Chr	Factor	Gene Expr.	Telomere State	Banding	Structural Var.	Health (%)
1	I (Altitude)	0.55	Steady (●)	Moderate, balanced	None	92
2	P (Slope)	0.42	Warning (▽)	Light, low-expression	None	74
3	D (Damping)	0.88	Fuse (▲)	Dark, high-expression	None (overload+)	85
4	S (Entropy)	0.18	Warning (▽)	Very light, deficiency	None	68
5	Dev-I (Equilibrium)	0.12	Warning (▽)	Very light, deficiency	None	65
6	Dev_1 (Mean rev.)	0.65	Steady (●)	Moderate	None	94
7	Dev_2 (Hist. sim.)	0.72	Fuse (▲)	Dark, high-predict.	None (overload+)	83
8	Dev_3 (Consensus)	0.38	Warning (▽)	Light, consensus-high	None	71
Drift Risk Score R (weights w_{sv}=0.4, w_{tel}=0.35, w_{trend}=0.25)						**15/100**

TABLE V: Offspring Distribution Statistics (Buffett×Soros, N=1,000)

Dim.	μ	m	σ	P_{25}	P_{75}	Δ
TOL	0.634	0.625	0.227	0.434	0.844	0.128
INF	0.832	0.837	0.099	0.766	0.904	0.003
VIS	0.760	0.758	0.134	0.659	0.870	0.062
SPD	0.558	0.562	0.270	0.315	0.806	0.173
ENT	0.592	0.599	0.179	0.449	0.739	0.002
LEAD	0.818	0.821	0.102	0.753	0.890	0.014

Simplified genetics. The Mendelian model assumes independent assortment and simple dominance, which are simplifications even in biological genetics. Epistasis, polygenic inheritance, and environmental effects are not modeled.

Single-case validation. The Moutai analysis demonstrates the pipeline but does not constitute a systematic evaluation across diverse asset classes. A multi-asset karyotype benchmark is needed.

No longitudinal validation. The telomere-shortening model (decision system aging) has not been validated against longitudinal data. This requires tracking the same decision system over multiple reporting periods.

C. Future Work

- Multi-asset karyotype benchmarking: apply the framework to 50+ stocks across different sectors and market caps to establish normative karyotype distributions;
- Telomere dynamics: model the relationship between telomere shortening rate and subsequent decision-quality degradation;
- Epigenetic layer: introduce environmental modifiers (market regime, policy changes, macro conditions) that alter gene expression without changing the underlying chromosome structure;
- Portfolio karyotype: extend from single-asset to portfolio-level karyotyping, where each holding is a chromosome and the portfolio is the "genome";
- InvestorBench integration: submit the framework to the InvestorBench benchmark [1] for standardized performance comparison;
- Cross-species genetics: extend the simulator to model "cross-species" personality inheritance (e.g., value investor × quant trader).

VIII. Conclusion

We have presented the Fibonacci–Chromosome Isomorphism framework—a novel cross-domain approach to financial decision diagnostics and personality genetics. The framework maps eight-dimensional financial vectors onto eight decision chromosomes, enabling karyotype analysis with automatic structural-variation detection. It further simulates cross-generational transmission of decision personalities through a Mendelian inheritance model with Fibonacci-positioned crossover hotspots. Validation through the Moutai full-pipeline analysis and the Buffett×Soros genetic simulation demonstrates the framework's practical utility and theoretical coherence. The Moutai karyotype reveals a "textbook-stable" configuration with zero structural variations, while the genetic simulation confirms the predicted dominance–recessiveness patterns. The framework is open-source, implemented in pure Python, and designed for extensibility. We believe the genomic-level diagnostic paradigm offers a compelling alternative to traditional black-box quantitative models, particularly in contexts where interpretability and structural understanding are paramount. As AI-driven financial decision-making continues to mature, frameworks that bridge the gap between numerical precision and human-interpretable structure will become increasingly valuable. The Fibonacci–Chromosome Isomorphism is a step in that direction.

Code Availability

The complete source code is available at:

- `chromosome_diagnostic.py` — Decision Chromosome Karyotyping Tool;
- `personality_genetics.py` — Personality Genetics Simulator.

Project website: https://hellomind-star.github.io/ymine/. Both scripts are implemented in pure Python (standard library only) and require no external dependencies.

Acknowledgment

We thank the Game-OS research community for feedback on earlier drafts. The DNA double-helix inspiration draws on the seminal work of Watson and Crick [12].

REFERENCES

[1] H. Li, Y. Cao, Y. Yu, S. R. Javaji, Z. Deng, Y. He, Y. Jiang, Z. Zhu, K. Subbalakshmi, G. Xiong, J. Huang, L. Qian, X. Peng, Q. Xie, and J. W. Suchow, "INVESTORBENCH: A benchmark for financial decision-making tasks with LLM-based agents," in *Proceedings of the 63rd Annual Meeting of the Association for Computational Linguistics (ACL)*, 2025.

[2] V. I. Yukalov and D. Sornette, "Mathematical structure of quantum decision theory," *Advances in Complex Systems*, vol. 13, no. 5, pp. 659–698, 2010.

[3] E. W. Piotrowski and J. Sładkowski, "Quantum market games," *Physica A: Statistical Mechanics and its Applications*, vol. 312, no. 1–2, pp. 208–216, 2002.

[4] R. Suzuki and T. Arita, "An evolutionary model of personality traits related to cooperative behavior using a large language model," *Scientific Reports*, vol. 14, no. 1, p. 5989, 2024.

[5] P. Han, R. Kocielnik, P. Song, R. Debnath, D. Mobbs, A. Anandkumar, and R. M. Alvarez, "The personality illusion: Revealing dissociation between self-reports and behavior in LLMs," *arXiv preprint arXiv:2509.03730*, 2025, neurIPS 2025 LAW Workshop (Best Paper Honorable Mention).

[6] Y. Yu, Z. Yao, H. Li, Z. Deng, Y. Jiang, Y. Cao, Z. Chen, J. W. Suchow, Z. Cui, R. Liu, Z. Xu, D. Zhang, K. Subbalakshmi, G. Xiong, Y. He, J. Huang, D. Li, and Q. Xie, "FinCon: A synthesized LLM multi-agent system with conceptual verbal reinforcement for enhanced financial decision making," in *Advances in Neural Information Processing Systems (NeurIPS)*, 2024.

[7] B. Zhang, K. Chen, J. Wang, X. Liu *et al.*, "FinPos: A position-aware trading agent system for real financial markets," *arXiv preprint arXiv:2510.27251*, 2025.

[8] Y. Xiao, E. Sun, D. Luo, and W. Wang, "TradingAgents: Multi-agents LLM financial trading framework," *arXiv preprint arXiv:2412.20138*, 2024, in Proceedings of the AAAI Conference on Artificial Intelligence.

[9] X.-Y. Liu, H. Yang, Q. Chen, R. Zhang, L. Yang, B. Xiao, and C. D. Wang, "FinRL: A deep reinforcement learning library for automated trading in quantitative finance," *arXiv preprint arXiv:2011.09607*, 2021, also in NeurIPS 2020 Deep RL Workshop.

[10] H. Rahman and S. Desai, "Behavior-adaptive conversational agents: Toward a fluid personality framework," *arXiv preprint arXiv:2607.01034*, 2026, presented at the AAAI 2026 Bridge Program on AI and Behavior Change.

[11] M. Livio, *The Golden Ratio: The Story of Phi, the World's Most Astonishing Number*. Broadway Books, 2002.

[12] J. D. Watson and F. H. C. Crick, "Molecular structure of nucleic acids: A structure for deoxyribose nucleic acid," *Nature*, vol. 171, pp. 737–738, 1953.